We are IntechOpen, the world's leading publisher of Open Access books Built by scientists, for scientists

6,900
Open access books available

185,000
International authors and editors

200M
Downloads

Our authors are among the

154
Countries delivered to

TOP 1%
most cited scientists

12.2%
Contributors from top 500 universities



WEB OF SCIENCE™

Selection of our books indexed in the Book Citation Index in Web of Science™ Core Collection (BKCI)

Interested in publishing with us?
Contact book.department@intechopen.com

Numbers displayed above are based on latest data collected.
For more information visit www.intechopen.com



2

Four-Wave Mixing in Silicon Nanowire Waveguides and Its Applications in Wavelength Conversion

Shiming Gao and Sailing He
Centre for Optical and Electromagnetic Research,
State Key Laboratory of Modern Optical Instrumentation,
Zhejiang University, Hangzhou,
China

1. Introduction

In recent years, silicon photonics has been considered as a new promising technology platform for low-cost optical communications and interconnects. Silicon photonic devices can be fabricated using existing semiconductor techniques. It has the possibility to integrate optical and electronic components onto a single microchip since silicon is already used as the substrate for most integrated circuits. Silicon nanowire waveguides based on silicon-on-insulator techniques have exhibited the high-density integration of optical circuits due to the strong light confinement from its high refractive-index contrast. Nowadays, the silicon nanowire waveguides can be easily fabricated with the accuracy of nanometer and the power density is higher than that of the conventional single-mode fiber by a factor of about 1000 (Fukuda et al., 2005). Therefore, nonlinear optical effects will easily occur although a low input power is used. On the other hand, the nonlinear Kerr coefficient of silicon is still high, which strengthens the nonlinear ability of silicon nanowire waveguides. Many kinds of nonlinear effects, such as self-phase modulation, cross-phase modulation, stimulated Raman scattering, two-photon absorption (TPA), and four-wave mixing (FWM), have been observed in silicon nanowire waveguides, and have been used to realize silicon Raman lasers (Boyraz & Jalali, 2004), Raman amplifiers (Liang & Tsang, 2004), all-optical switches (Almeida et al., 2004), logical gates (Liang et al., 2006), parametric amplifiers (Foster et al., 2006), and wavelength converters (Rong et al., 2006).

In particular, wavelength conversion is an essential operation in wavelength-routing wavelength division multiplexing networks and FWM in silicon nanowire waveguides has been regarded as a promising alternative due to the all-optical and strictly transparent characteristics, etc. Wavelength conversion has been realized in silicon nanowire waveguides using coherent anti-Stokes Raman scattering (Raghunathan et al., 2005) or nonresonant electronic response FWM (Lin et al, 2006). For a real-life wavelength converter, conversion efficiency and bandwidth are two important figures of merit. In addition, polarization dependency will also influence the performance of wavelength converters. Different from the wavelength conversion in optical fibers, the nonlinear losses due to TPA and TPA-induced free-carrier absorption (FCA) will greatly affect the conversion efficiency in silicon nanowire waveguides (Sang & Boyraz, 2008), especially where the FCA effect is quadratically proportional to the incident power.

In this chapter, the theoretical model of FWM in silicon nanowire waveguides will be introduced by taking into account all the factors including self-phase modulation, cross-phase modulation, TPA, and TPA-induced FCA. The progresses on the bandwidth enhancement will be reviewed by engineering the dispersion profile of the silicon nanowire waveguide through changing the waveguide geometry or designing special waveguide structures, as the phase-matching condition of the FWM effect is tightly dominated by the waveguide dispersion. Also, the bandwidth can be enhanced by introducing two-pump regimes and realizing wavelength conversion via nondegenerate FWM. FWM based wavelength conversion is tightly related to the state of polarization (SOP) of the input signal with respect to the pump. In particular, no converted signal can be generated if they are polarized orthogonally to each other. The realization of polarization independency of wavelength conversion in silicon nanowire waveguides will also be reviewed to eliminate the influence of the polarization of the input signal wave.

2. Theoretical model of FWM in silicon nanowire waveguides

FWM in silicon nanowire waveguides can be classified as degenerate and nondegenerate FWMs according to the number of the incident pumps. Degenerate FWM efficiently occurs when a single pump wave λ_p is injected into a silicon nanowire waveguide together with a signal wave λ_s when the phase-matching condition is well satisfied. A converted wave λ_c is generated under the energy conservation condition $1/\lambda_c = 2/\lambda_p - 1/\lambda_s$. By taking the linear propagation loss, TPA, and FCA into account, the coupled equations for the FWM process under the continuous wave or quasi-continuous wave assumption can be expressed as (Zhang et al., 2009)

$$\frac{dA_p}{dz} = -\frac{1}{2}\left(\alpha_p + \alpha_{TPAp} + \alpha_{FCAp}\right)A_p + j\gamma_p\left[\left|A_p\right|^2 + 2\left|A_s\right|^2 + 2\left|A_c\right|^2\right]A_p + 2j\gamma_p A_p^* A_s A_c \exp(j\Delta\beta z) \quad (1)$$

$$\frac{dA_s}{dz} = -\frac{1}{2}\left(\alpha_s + \alpha_{TPAs} + \alpha_{FCAs}\right)A_s + j\gamma_s\left[2\left|A_p\right|^2 + \left|A_s\right|^2 + 2\left|A_c\right|^2\right]A_s + j\gamma_s A_c^* A_p^2 \exp(-j\Delta\beta z) \quad (2)$$

$$\frac{dA_c}{dz} = -\frac{1}{2}\left(\alpha_c + \alpha_{TPAc} + \alpha_{FCAc}\right)A_c + j\gamma_c\left[2\left|A_p\right|^2 + 2\left|A_s\right|^2 + \left|A_c\right|^2\right]A_c + j\gamma_c A_s^* A_p^2 \exp(-j\Delta\beta z) \quad (3)$$

For the nondegenerate FWM, two pumps λ_{p1} and λ_{p2} are injected into the silicon nanowire waveguide together with the signal λ_s. A converted wave λ_c is generated at $1/\lambda_c = 1/\lambda_{p1} + 1/\lambda_{p2} - 1/\lambda_s$. The coupled equations can be expressed as (Gao et al., 2010)

$$\begin{aligned}\frac{dA_{p1}}{dz} = &-\frac{1}{2}\left(\alpha_{p1} + \alpha_{TPAp1} + \alpha_{FCAp1}\right)A_{p1} + j\gamma_{p1}\left[\left|A_{p1}\right|^2 + 2\left|A_{p2}\right|^2 + 2\left|A_s\right|^2 + 2\left|A_c\right|^2\right]A_{p1} \\ &+ 2j\gamma_{p1}A_{p2}^* A_s A_c \exp(j\Delta\beta z)\end{aligned} \quad (4)$$

$$\begin{aligned}\frac{dA_{p2}}{dz} = &-\frac{1}{2}\left(\alpha_{p2} + \alpha_{TPAp2} + \alpha_{FCAp2}\right)A_{p2} + j\gamma_{p2}\left[2\left|A_{p1}\right|^2 + \left|A_{p2}\right|^2 + 2\left|A_s\right|^2 + 2\left|A_c\right|^2\right]A_{p2} \\ &+ 2j\gamma_{p2}A_{p1}^* A_s A_c \exp(j\Delta\beta z)\end{aligned} \quad (5)$$

$$\frac{dA_s}{dz} = -\frac{1}{2}\left(\alpha_s + \alpha_{TPAs} + \alpha_{FCAs}\right)A_s + j\gamma_s\left[2\left|A_{p1}\right|^2 + 2\left|A_{p2}\right|^2 + \left|A_s\right|^2 + 2\left|A_c\right|^2\right]A_s + 2j\gamma_s A_c^* A_{p1} A_{p2}\exp(-j\Delta\beta z) \tag{6}$$

$$\frac{dA_c}{dz} = -\frac{1}{2}\left(\alpha_c + \alpha_{TPAc} + \alpha_{FCAc}\right)A_c + j\gamma_c\left[2\left|A_{p1}\right|^2 + 2\left|A_{p2}\right|^2 + 2\left|A_s\right|^2 + \left|A_c\right|^2\right]A_c + 2j\gamma_c A_s^* A_{p1} A_{p2}\exp(-j\Delta\beta z) \tag{7}$$

In Eqs. (1)-(7), $A_{p,p1,p2,s,c}(z)$ are the amplitudes of the pumps, the signal, and the converted waves, $\gamma_{p,p1,p2,s,c}$ are the nonlinear coefficients, $\Delta\beta$ is the linear phase mismatch, $a_{p,p1,p2,s,c}$ are the linear-loss coefficients, $a_{TPAp,p1,p2,s,c}$ and $a_{FCAp,p1,p2,s,c}$ are the nonlinear-loss coefficients caused by the TPA and FCA effects. Mathematically the loss coefficients induced by TPA and FCA can be expressed as

$$\alpha_{TPAi} = \frac{\beta_{TPA}}{A_{eff}}\left(\left|A_i\right|^2 + 2\sum_{m\neq i}\left|A_m\right|^2\right),$$

($i,m = p,s,c$ for single-pump FWM; $i,m = p1,p2,s,c$ for two-pump FWM) (8)

$$\alpha_{FCAi} = \frac{\sigma_i\beta_{TPA}\tau}{2hcA_{eff}^2}\left(\sum_m \lambda_m\left|A_m\right|^4 + 4\sum_{m\neq n}\frac{\lambda_m\lambda_n\left|A_m\right|^2\left|A_n\right|^2}{\lambda_m + \lambda_n}\right),$$

($i,m = p,s,c$ for single-pump FWM; $i,m = p1,p2,s,c$ for two-pump FWM) (9)

where $\sigma_{p,p1,p2,s,c}$ are the FCA cross sections.
Denoting the nonlinear index coefficient of silicon as n_2, the nonlinear coefficients for the involved waves can be calculated as

$$\gamma_i = 2\pi n_2 / \lambda_i A_{eff}\ , \quad (i = p,p1,p2,s,c) \tag{10}$$

Since all the involved waves are in the same wavelength region, it is reasonable to consider $a_{p,p1,p2,s,c} = a$, $\sigma_{p,p1,p2,s,c} = \sigma$, and $\gamma_{p,p1,p2,s,c} = \gamma$. Supposing $P_{p,p1,p2,s,c} = |A_{p,p1,p2,s,c}|^2$ the phase mismatch can be reduced to a simple expression for single-pump FWM (Foster et al., 2007):

$$\kappa_d = \Delta\beta + 2\gamma P_p = \beta_s + \beta_c - 2\beta_p + 2\gamma P_p \tag{11}$$

And for the two-pump FWM:

$$\kappa_{nd} = \Delta\beta + \gamma\left(P_{p1} + P_{p2}\right) = \beta_s + \beta_c - \beta_{p1} - \beta_{p2} + \gamma\left(P_{p1} + P_{p2}\right) \tag{12}$$

where $\beta_{p,p1,p2,s,c}$ are the wave numbers of the interacting waves.
In lossy cases and saturation regimes only numerical solutions are available for Eqs. (1)-(3) or Eqs. (4)-(7). In particular the solution to Eq. (3) or Eq. (7) leads to the definition of the conversion efficiency and the conversion bandwidth. The calculation of conversion efficiency, which is defined as

$$\eta(dB) = 10\log_{10}\left[P_c(z) / P_s(0)\right] \tag{13}$$

provides an easy solution to the determination of the conversion bandwidth after solving the coupled equations numerically.

3. Wavelength conversion based on FWM in silicon nanowire waveguides

FWM is considered to be an effective way to realize all-optical and strictly transparent wavelength conversion. In this section, the applications of FWM in silicon nanowire waveguides on wavelength conversion will be introduced, including bandwidth enhancement, efficiency improvement, and polarization independency.

3.1 Bandwidth enhancement and efficiency improvement of FWM-based wavelength conversion

Conversion bandwidth and efficiency are two important performances for wavelength conversion in dense wavelength division multiplexing systems. For FWM-based wavelength conversion, the conversion bandwidth is dominated by the phase-matching condition. Since the phase mismatch is effectively changed by the dispersion profile and the pump wavelength setting, it is reasonable to realize broadband wavelength conversion through dispersion engineering or two-pump regime.

3.1.1 Optimization of waveguide geometry

The conversion bandwidth is dominated by the dispersion property of the waveguide since it determines the linear phase mismatch of the involved waves. The linear phase mismatch can be considered as the contribution of two parts: one is the material dispersion, which is large and normal within the telecommunication wavelength range; and the other is the waveguide dispersion, which can vary from anomalous to normal by adjusting the waveguide dimensions (Turner et al., 2006). Considering a silicon channel wavegudie, Fig. 1 shows the values of the zero-dispersion wavelength (ZDW) corresponding to different waveguide sizes. Generally, there are two ZDWs in the entire wavelength region and both of them shift to the long wavelength for TE mode as the waveguide dimensions increase. For TM mode, the left ZDW shifts first to the short and then to the long wavelength and the right ZDW keeps increasing as the waveguide dimensions increase. Figures 1(a) and 1(b) show the distribution of the left and the right ZDWs for TE mode in terms of the waveguide dimensions, respectively. Figures 1(c) and 1(d) are for TM mode. The available wavelength range is considered from 1300 to 2000 nm (shown as the colorful zone in Fig. 1). The white zone in Fig. 1 indicates that there is no ZDW within this wavelength range.

In order to avoid the influence of higher-order modes on the FWM process, the nanowire waveguide is required to be of single mode. The single-mode condition for the waveguides at a specific wavelength of 1550 nm is numerically analyzed by using the semi-vectorial beam propagation method. To obtain the single-mode condition, one can scan the height and width of the silicon nanowire waveguide and judge whether higher-order modes exist. For a fixed height we reduce the width with a step of 5 nm until all the higher-order modes disappear. The calculated results are also shown in Fig. 1. The solid curves indicate the critical boundaries of single mode for TE mode in Figs. 1(a) and 1(b), and the curves are for TM mode in Figs. 1(c) and 1(d). The single-mode region is on the left-bottom side of the curve and the multi-mode region is on the right-top side in each figure.

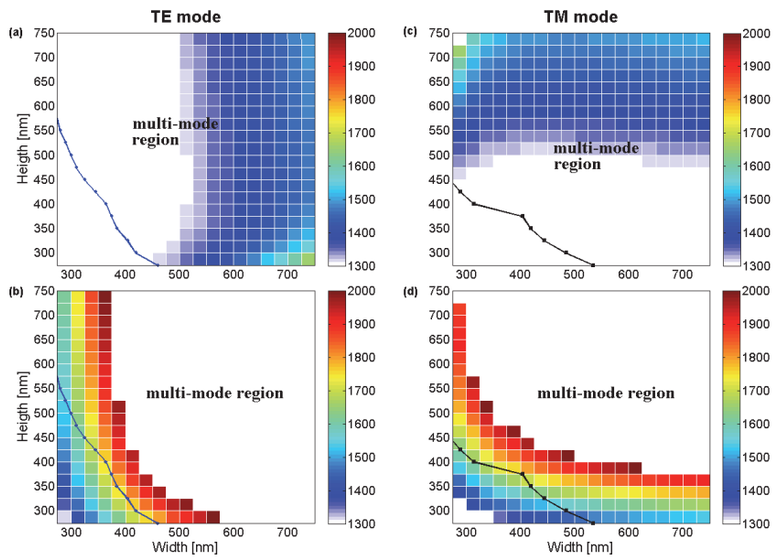


Fig. 1. Distribution of the ZDWs for the TE and TM modes. (a) the left ZDW for TE mode; (b) the right ZDW for TE mode; (c) the left ZDW for TM mode; (d) the right ZDW for TM mode. The solid lines in (a)-(d) denote the single-mode conditions for TE or TM modes. (Zhang et al., 2009 ; © 2009 The Electromagnetics Academy)

The dispersion profile of the silicon channel waveguide is directly determined by the waveguide geometry. By selecting suitable waveguide height and width, the ZDW can be shifted to the 1550-nm region and the dispersion can be flattened. Figure 2 shows the dispersion versus the wavelength for some waveguides whose ZDWs are all around 1555 nm. For the TE mode, the dispersion slope increases as the waveguide height increases. The situation is reversed for the TM mode. The flatter the curve is, the broader the conversion bandwidth is since the phase mismatch of the involved waves maintains small values within a wide wavelength range. After comparing the dispersion slopes of these waveguides, the waveguide cross section is optimized as 400 nm × 269 nm (height × width) for the TM mode in order to obtain the smallest dispersion slope corresponding to the broadest conversion bandwidth.

Figure 3(a) shows the conversion efficiency versus the wavelength detuning for different pump wavelengths in the anomalous region in the optimized waveguide of 400 nm × 269 nm with a fixed input power of 200 mW, a = 2.5 dB/cm, σ = 1.45 × 10^{-17} cm^2, β_{TPA} = 0.3 cm/GW, and τ = 1 ns. When the pump is tuned away from the ZDW, the appearance of a second pair of conversion efficiency peaks farther from the pump, which is introduced by the location shift and increased number of the perfect phase-matching wavelengths, increases the 3-dB bandwidth. The maximum conversion bandwidth is achieved when the pump is at 1538.7 nm with the assumption of a 200-mW input pump power and a 2-cm-long interaction length. Figure 3(b) simulates the conversion response for the optimized 400 nm × 269 nm waveguide for TM polarization together with two other waveguides with the dimensions of 275 nm × 351 nm for TE polarization and 375 nm × 287 nm for TM polarization. These results are obtained in a 2-cm-long waveguide with a 200-mW pump wave at 1538.7 nm. The 3-dB bandwidth is over 280 nm for the optimized waveguide and the bandwidths of 275 nm × 351 nm and 375 nm × 287 nm waveguides are 77 nm and 112 nm.

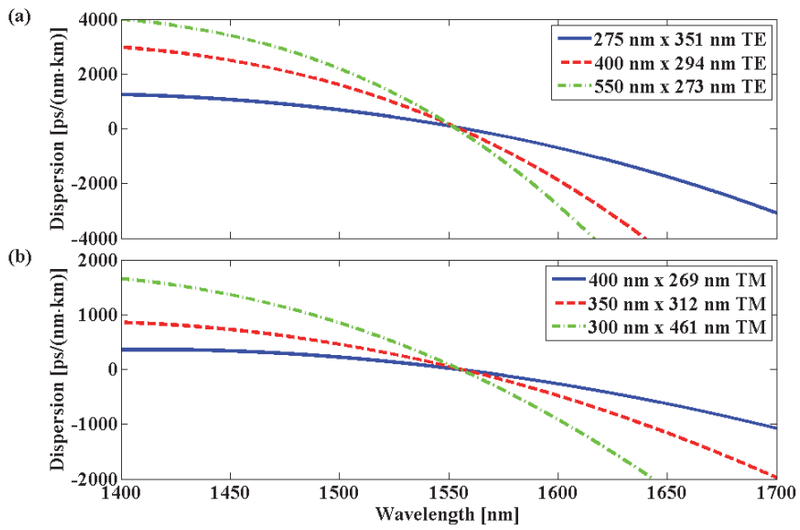


Fig. 2. Dispersion as a function of the wavelength for (a) TE and (b) TM modes. (Zhang et al., 2009 ; © 2009 The Electromagnetics Academy)

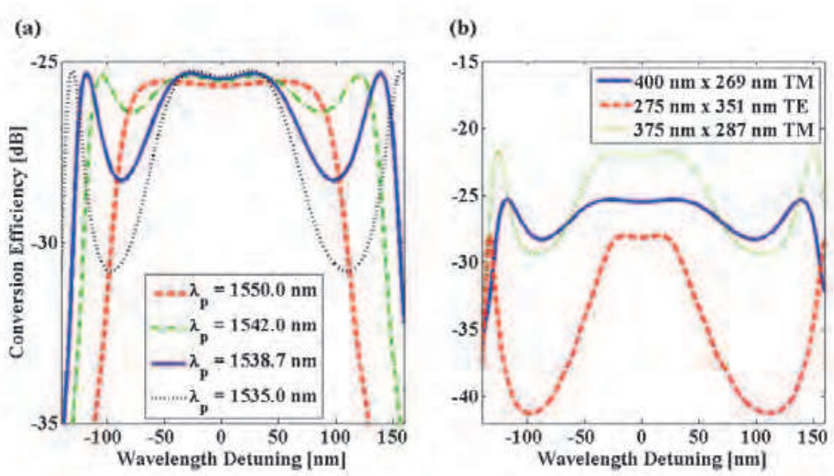


Fig. 3. (a) Conversion efficiency versus the wavelength detuning for different pump wavelengths in the optimized 400 nm × 269 nm waveguide. (b) Conversion response comparison of the 400 nm × 269 nm, 275 nm × 351 nm, and 375 nm × 287 nm waveguides with the optimized pump wavelength. (Zhang et al., 2009 ; © 2009 The Electromagnetics Academy)

3.1.2 Design of slot waveguide structure

The efficiency of FWM is tightly related to the nonlinear coefficient of the silicon nanowire waveguide. If the field is effectively confined to decrease the effective mode area, the nonlinear coefficient can be increased (Liu et al., 2011). Figure 4(a) shows a schematic description of the silicon slot waveguide filled with silicon nanocrystals (Si-nc's). This kind of Si-nc material has a high Kerr coefficient at telecommunication wavelengths and its fabrication is compatible with the conventional semiconductor technologies (Martínez et al., 2010). By assuming that the Si-nc's have a silicon excess of 0.08 and a linear refractive index

of 1.6, a typical transverse electronic (TE) mode distribution is shown in Fig. 4(b), where the slot width is assumed to be W_s = 50 nm, the silicon slab width is W_h = 310 nm, and the waveguide height is h = 305 nm. From Fig. 4(b) one can find that the field is strongly confined in the low index nonlinear material due to the high index contrast in the horizontal direction. The effective mode area is calculated to be 0.042 μm² at 1550 nm. By using the definition in Eq. (10), the corresponding nonlinear coefficient is calculated to be γ = 3.86 × 10^6 $W^{-1}km^{-1}$. For comparison, the mode area and nonlinear coefficient are calculated to be 0.15 μm² and 1.53 × 10^5 $W^{-1}km^{-1}$ for a 305 nm × 670 nm silicon channel waveguide, which has approximately the same dimensions as the slot waveguide above. The nonlinear coefficient of the slot waveguide is roughly 19 times larger than that of the channel waveguide, which means higher conversion efficiency, due to both the high confinement of the light in the slot structure and the high nonlinearity of Si-nc's.

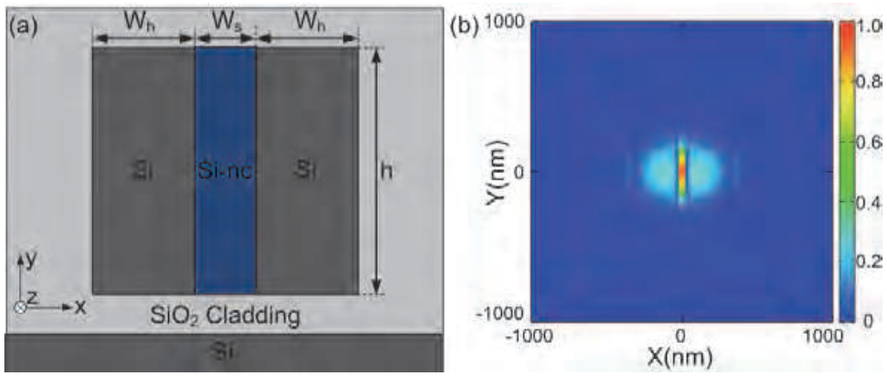


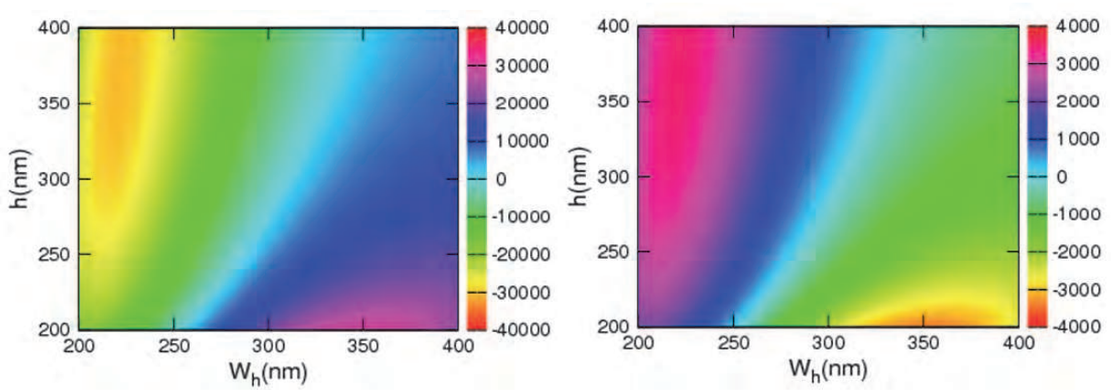
Fig. 4. (a) Schematic configuration of a slot waveguide, (b) Mode profile of the slot waveguide structure calculated by the beam propagation method. (Liu et al., 2011; © 2011 OSA)

As shown in Eq. (11), the phase-matching condition is a dominating factor of the bandwidth in a FWM-based wavelength conversion and the linear phase mismatch $\Delta\beta$ is determined by the dispersion profile of the used waveguide. By expanding $\beta_{s,c}$ as the Taylor series to the fourth-order around the pump frequency ω_p and omitting the higher-order items, the linear phase mismatch can be rewritten as (Foster et al., 2007):

$$\begin{aligned}\Delta\beta &= \beta_2(\omega_p)\Omega^2 + \frac{1}{12}\beta_4(\omega_p)\Omega^4 \\ &= -\frac{1}{2\pi c}\lambda_p^2 D(\lambda_p)\Omega^2 - \frac{\lambda_p^4}{(2\pi c)^3}\left[\frac{1}{2}D(\lambda_p) + \frac{1}{2}\lambda_p D'(\lambda_p) + \frac{1}{12}\lambda_p^2 D''(\lambda_p)\right]\Omega^4\end{aligned} \tag{14}$$

where $\Omega = \omega_s - \omega_p$ is the frequency difference between the signal and pump waves. The linear phase mismatch is approximately determined by the dispersion and its first- and second-order derivatives at the pump wavelength. It is expected to realize the optimal bandwidth by scanning the waveguide parameters to acquire a minimal phase mismatch with a given frequency difference. Since the slot width W_s has very slight influence, it is reasonable to consider a fixed slot width to simplify the optimization. Here the slot width is chosen to be W_s = 50 nm (considering the limit of the fabrication technology). Figure 5(a) shows the variation of the linear phase mismatch in terms of h and W_h when the slot width is fixed to 50 nm. Here the pump and signal wavelengths are set to be 1550 and 1450 nm,

respectively. A set of zero points can be obtained for different waveguide heights h ranging from 200 to 400 nm when the slab width W_h is carefully chosen. For comparison, Fig. 5(b) shows the dispersion values at 1550 nm versus the waveguide dimensions. By comparing Fig. 5(a) with Fig. 5(b), one can find that the minimum absolute value of the linear phase mismatch agrees well with the ZDWs in the 1550-nm region for different waveguide dimensions, which means that the conversion bandwidth can be broadened further near the ZDW in the slot waveguide as long as the dispersion is flat enough. Among the designs with a minimum absolute value of the linear phase mismatch as well as a ZDW at 1550 nm in Fig. 5, an optimized waveguide configuration with W_h = 310 nm and h = 305 nm is found. The Si-nc slot waveguide with a 310-nm slab width, a 305-nm height, and a 50-nm slot width, whose mode area is about 0.042 μm², can be considered as an optimized structure to enhance the bandwidth of FWM-based wavelength conversion in 1550-nm wavelength window since it has smaller and flatter dispersion to satisfy the phase-matching condition.

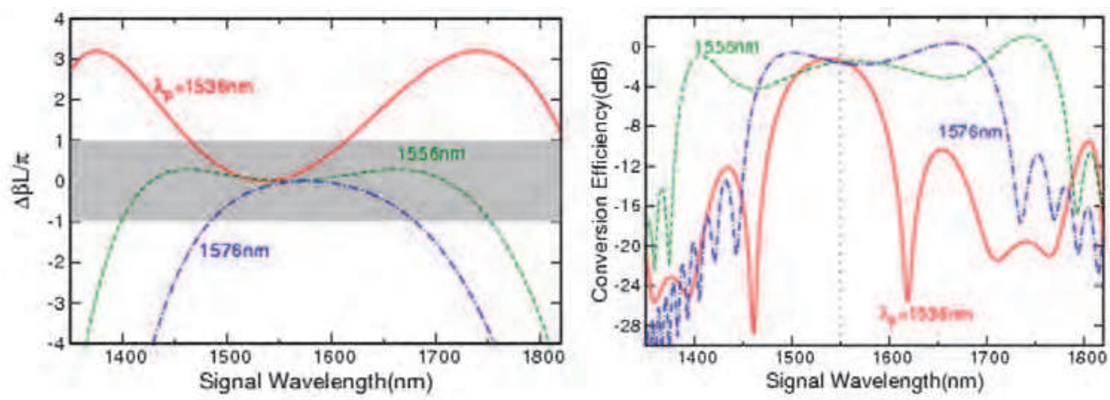


(a) (b)

Fig. 5. (a) Linear phase mismatch (in units of m^{-1}) as a function of h and W_h with W_s = 50 nm, (b) the dispersion value (in units of ps/km/nm) at 1550 nm as a function of h and W_h with W_s = 50 nm. (Liu et al., 2011; © 2011 OSA)

After optimizing the dispersion of the Si-nc slot waveguide, the performance of FWM-based wavelength conversion is evaluated in such a waveguide by comparing with some traditional silicon nanowire waveguides. Assuming that all the pump, signal, and idler waves are polarized along the TE-axis, the coupled equations for the single-pump FWM process can be expressed using Eqs. (1)-(3). Assuming that the parameter values are as follows: $n_2 = 4 \times 10^{-17}$ m^2/W, $\beta_{TPA} = 5 \times 10^{-11}$ m/W, τ_{eff} = 1 ns, $a_{p,s,i}$ = 6 dB/cm, and $\sigma_{p,s,i} = 3.5 \times 10^{-22}$ m^2, one can obtain the conversion efficiency by numerically solving these coupled equations. When a continuous-wave (cw) pump with a power of 150 mW and a signal with a power of 15 mW are used, Fig. 6(a) shows the linear phase mismatch as a function of the signal wavelength for three different pump wavelengths including 1536, 1556, and 1576 nm in a 6-mm-long optimized Si-nc slot waveguide (W_h = 310 nm, W_s = 50 nm, and h = 305 nm). The phase mismatch is tightly connected to the pump wavelength and it can be effectively controlled within a small value by setting the pump in the anomalous dispersion region near the ZDW (1550 nm). Correspondingly, the conversion responses for the three different pumps are simulated in Fig. 6(b) in the 6-mm-long slot waveguide. The two side peaks on conversion efficiency correspond

to the two zero points far away from the ZDW, where the phase-matching condition is also satisfied. From Fig. 6(b), the conversion bandwidth can be read out to be 87, 390, and 250 nm for the 1536-, 1556-, and 1576-nm pumps, respectively. The conversion bandwidth reaches its maximum with the 1556-nm pump.



(a) (b)

Fig. 6. (a) Linear phase mismatch and (b) conversion efficiency as the signal wavelength varies for three pumps at 1536, 1556, and 1576 nm in a 6-mm-long waveguide. (Liu et al., 2011; © 2011 OSA)

The conversion bandwidth will reduce as the waveguide length increases since the accumulated phase mismatch is proportional to the waveguide length. Also, the conversion efficiency is influenced by the waveguide length. Figure 7 simultaneously shows the conversion bandwidth and the efficiency as functions of the waveguide length for the slot waveguide as well as for a traditional silicon channel waveguide (280 nm × 342 nm), which also has an optimized dispersion profile with ZDW at 1550 nm. The pump and signal powers are assumed to be 150 and 15 mW and the pump wavelengths of the slot and channel waveguide are set to be 1556 and 1535 nm to obtain broader conversion bandwidths. For both waveguides, the conversion bandwidth remarkably drops as the waveguide becomes longer. The bandwidth decreases form 407 to 83 nm for the slot waveguide or from 271 to 101 nm for a silicon channel waveguide when the waveguide length increases form 4 to 20 mm. The two discontinuities in the bandwidth curves of these two waveguides are caused by the two concavities beside the pump wavelength in the conversion efficiency curves (Zhang et al., 2009). The conversion bandwidth of a slot waveguide is greatly broader than a traditional channel waveguide when the waveguide is short while it is a little narrower when the waveguide length increases. However, the conversion efficiency of the slot waveguide is much higher than that of the traditional channel waveguide, which reaches -1.46 dB when the waveguide is 7 mm long. The conversion efficiency for the silicon channel waveguide can reach -16.6 dB in the 20-mm-long waveguide, which is nearly 15 dB lower than the slot waveguide under the same incident condition. As shown in Fig. 7, a 3-dB conversion bandwidth of over 400 nm incorporating a conversion efficiency of -2.38 dB can be achieved in a 4-mm-long slot waveguide.

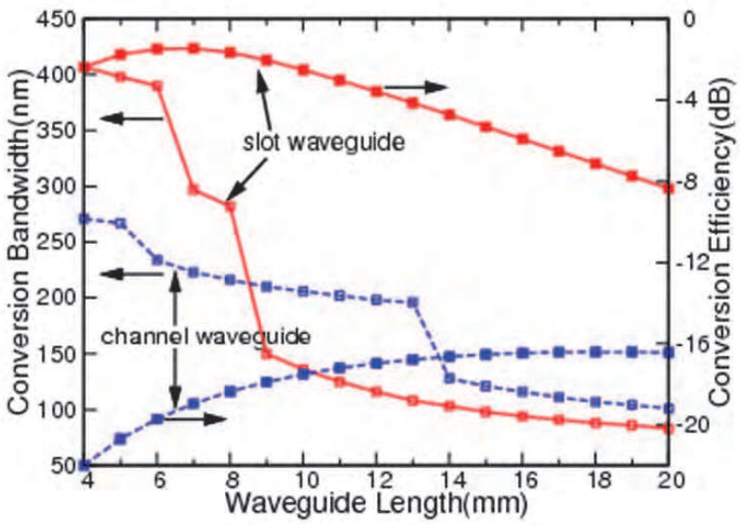


Fig. 7. Conversion bandwidth and efficiency as the waveguide length varies for the slot waveguide and the silicon channel waveguide. (Liu et al., 2011; © 2011 OSA)

3.1.3 Usage of two-pump FWM

According to Eq. (12), the phase-matching condition of FWM can be freely controlled by the pump spacing when a two-pump regime is used and the bandwidth may be enhanced by setting the pumps. Preliminary calculations are performed in a 1.5-cm-long 300 nm × 650 nm silicon nanowire waveguide that corresponds to a 0.12158 μm² effective mode area. The zero-dispersion wavelength is at 1456 nm. Since the pump power attenuates along the propagation length, the phase mismatch will vary with respect to the distance even though the signal wavelength is fixed. For the single-pump FWM-based wavelength conversion, Fig. 8(a) and 8(b) simulate the phase mismatches for the pump powers of 100 mW and 1000 mW in the above waveguide and the pump wave is assumed to be set at 1550 nm. In our calculation, the linear propagation loss coefficient is assumed to be α = 2.5 dB/cm, the TPA coefficient is β_{TPA} = 0.8 cm/GW for both degenerate and nondegenerate absorptions, the FCA cross section is $\sigma = 1.45 \times 10^{-17}$ cm², the effective free-carrier lifetime of carriers is τ = 2 ns, and the nonlinear index coefficient is $n_2 = 9 \times 10^{-18}$ m²/W. One can see that the exact phase-matching curves in Figs. 8(a) and 8(b) are quite similar particularly after propagating 0.5 cm in the silicon nanowire waveguide, although the incident pump powers are dramatically different. This effect results in the nonlinear loss due to TPA and FCA, especially where FCA is quadraticly proportional to the pump powers. A high incident power will be attenuated rapidly to a relatively low level. As a result, the phase mismatch is slightly changed by the pump power. Figure 8(c) shows the conversion responses for the two cases corresponding to Figs. 8(a) and 8(b) with a signal power of 1 mW. The 3-dB conversion bandwidths are 71.5 and 77.2 nm when 100-mW and 1000-mW pumps are adopted. The bandwidth enhancement is very limited by changing the pump power.

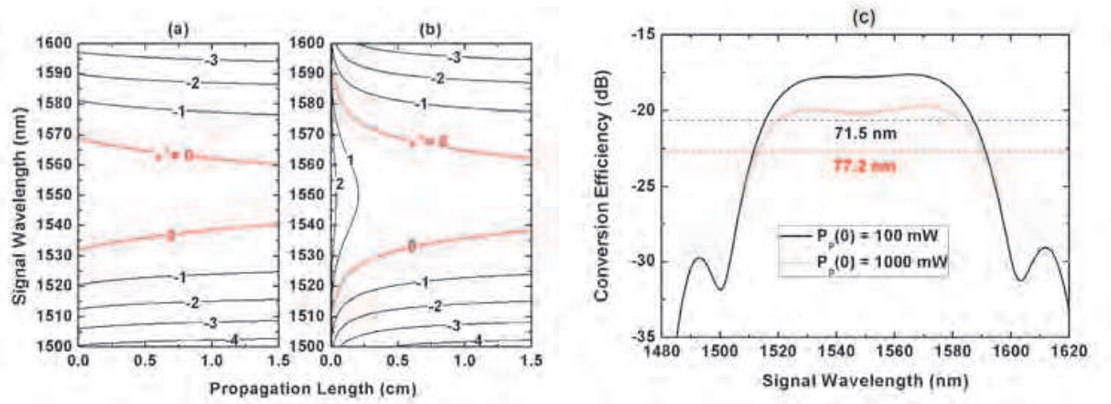


Fig. 8. Phase mismatch (in the units of cm^{-1}) of the single-pump FWM as a function of the signal wavelength and the propagation length with the pump power of (a) 100 mW or (b) 1000 mW. (c) Single-pump conversion efficiency as the signal wavelength for the pump power of 100 mW or 1000 mW. (Gao et al., 2010; © 2010 IEEE)

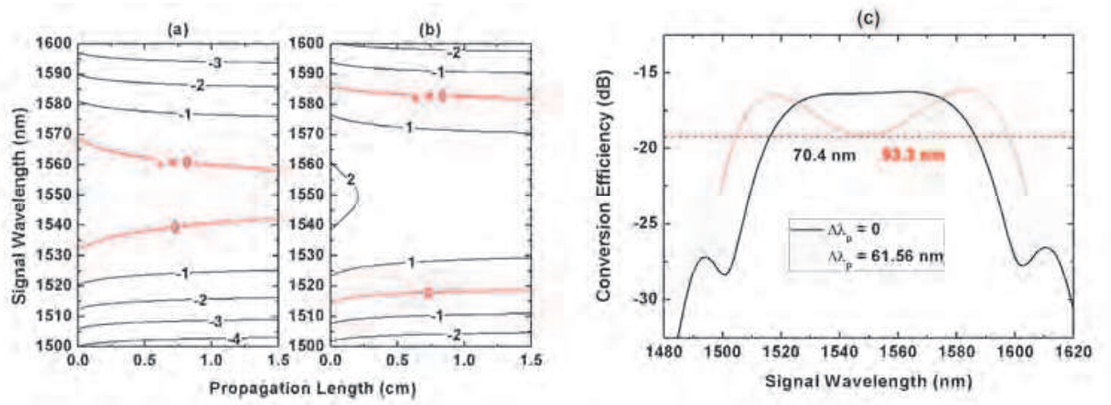


Fig. 9. Phase mismatch (in the units of cm^{-1}) of the two-pump FWM as a function of the signal wavelength and the propagation length when the wavelength spacing between the two pumps is (a) 0 and (b) 61.56 nm. (c) Two-pump conversion efficiency as the signal wavelength varies for the pump wavelength spacing of 0 or 61.56 nm. (Gao et al., 2010; © 2010 IEEE)

In contrast, the phase mismatch is greatly dependent on the two pump wavelengths in the two-pump FWM scheme. When the mean pump wavelength is fixed at 1550 nm, the phase mismatch is calculated by using Eq. (12) with a pump spacing of 0 and 61.56 nm, as shown in Figs. 9(a) and 9(b), in which the pump powers are fixed at 100 mW. The linear phase mismatch $\Delta\beta$ is directly determined by the pump wave numbers, that is, the pump wavelengths. One can find that the total phase mismatch is sensitive to the pump wavelength spacing and the perfect phase-matching curves (κ = 0) are separated from each other in the contour map as the pump spacing increases, which results in the enhancement of bandwidth. The simulation results of the conversion responses are shown in Fig. 9(c). The 3-dB bandwidth is 70.4 nm when the two pumps are very close, which is quite similar to the single-pump FWM. When the two pumps are separated from each other, the bandwidth is enhanced gradually. For the pump wavelength spacing of 61.56 nm, the bandwidth reaches 93.3 nm, which is enhanced by 22.9 nm (33%) compared to the case when the two pumps are put closely.

The nonuniformity of the conversion response is also concomitantly enhanced as the pump spacing of the two-pump FWM increases since the central signals suffer from larger phase mismatch, which means a lower conversion efficiency. For the sake of convenience, we define the efficiency difference between the maximum efficiency and the central minimum efficiency as the response nonuniformity. With both pump powers of 100 mW, the conversion bandwidth and the corresponding response nonuniformity are quantitatively simulated as the pump wavelength spacing varies, as shown in Fig. 10. One can see that the response nonuniformity is also enhanced together with the conversion bandwidth by separating the two pumps. The response nonuniformity reaches 3 dB for a 61.56-nm wavelength spacing. Further increasing the pump spacing results in a response nonuniformity of more than 3 dB and the 3-dB bandwidth is divided into two regions. Also, the conversion bandwidth will decrease as the pump spacing increases, which is not beneficial to the wavelength conversion function. The maximum 3-dB bandwidth of 93.3 nm can be achieved just when the response nonuniformity is 3 dB.

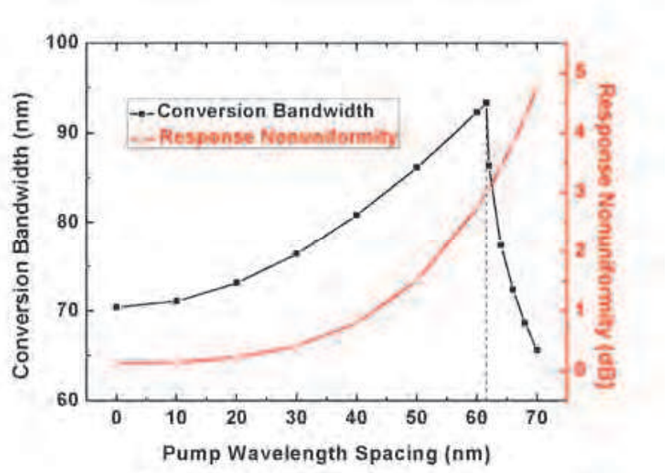


Fig. 10. Conversion bandwidth and the corresponding response nonuniformity as the pump wavelength spacing varies. (Gao et al., 2010; © 2010 IEEE)

The bandwidth enhancement based on two-pump FWM is experimentally demonstrated, as shown in Fig. 11. The two pumps are provided by two cw tunable lasers (Santec ECL-200) whose wavelengths are set at 1549.9 and 1564.8 nm. They are coupled through a 50/50 coupler and amplified using a high-power erbium-doped fiber amplifier (Amonics AEDFA-C-33-R), whose saturation power is around 23 dBm. The two pumps are filtered out through a demultiplexer whose central wavelength is at 1550 nm and a tunable band-pass filter, which is tuned to about 1565 nm. Another cw tunable laser (ECL-210) serves as the signal, whose output power is about 11 dBm. The pumps and signal are coupled into a 1.7-cm-long silicon waveguide with a cross section of 3 μm × 3 μm (the effective mode area is about 5 μm^2) via a 70/30 coupler. After this coupler, the powers of the two pumps and the signal are estimated to be around 13.2, 19.8, and 6.1 dBm, respectively. The coupling loss between the fiber and the waveguide is about 1.5 dB. In the silicon waveguide, FWM occurs among the two pumps and the signal, and an idler is generated. The FWM spectrum is observed using an optical spectrum analyzer (Ando AQ6317B).

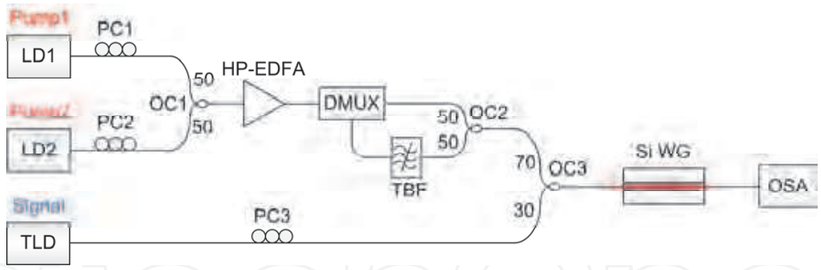


Fig. 11. Experimental setup for the wavelength conversion based on two-pump FWM. TLD: tunable laser diode, PC: polarization controller, EDFA: erbium-doped fiber amplifier, TBF: tunable bandwidth filter, OC: optical coupler, and OSA: optical spectrum analyzer. (Gao et al., 2010; © 2010 OSA)

Figure 12(a) shows the measured optical spectrum of the two-pump wavelength conversion using the experimental setup in Fig. 11. Here the signal is set at 1561.4 nm and the idler is generated at 1553.2 nm, which is enlarged and shown in the inset. From Fig. 12(a), one can find that the extinction ratio of the generated idler, which is defined as the difference between peak power and the noise floor, is about 10 dB with a measured resolution of 0.01 nm. For comparison, the FWM with a single pump is also experimentally demonstrated. Here Pump1 is turned off and Pump2 is tuned to 1557.7 nm, almost equal to the central wavelength of the two pumps in the two-pump FWM. As shown in Fig. 12(b), a signal at 1561.5 nm is converted to 1553.9 nm pumped by the single Pump2.

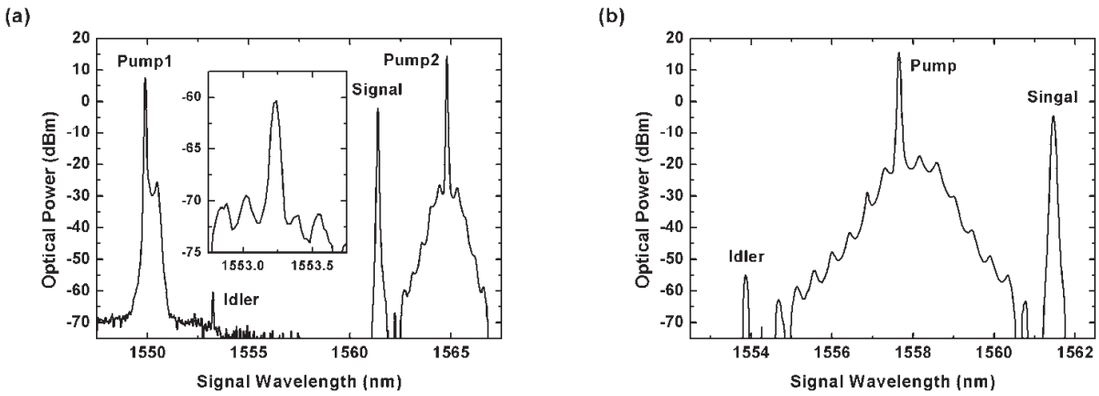


Fig. 12. (a) Optical spectrum of the FWM pumped by two cw pumps at 1549.9 nm and 1564.8 nm. The inset is the enlarged description of the generated idler. (b) Optical spectrum of the FWM pumped by a single cw pump at 1557.7 nm. (Gao et al., 2010; © 2010 OSA)

By scanning the signal wavelength, the response of conversion efficiency can be obtained from a series of measured FWM spectra, as shown in Fig. 13. It is known that the efficiency is tightly related to the pump powers, i.e., $\eta_{nd} \propto P_{p1}P_{p2}$ and $\eta_d \propto P_p^2$. In the experiments, the gains in the EDFA will be different for the two-pump and single-pump cases. For comparison, unit conversion efficiency is introduced by eliminating the influence of the pump powers (i.e., $\eta_{nd\text{-}unit} = \eta_{nd}/P_{p1}P_{p2}$ and $\eta_{d\text{-}unit} = \eta_d/P_p^2$). By fitting the measured conversion efficiencies, the experimental bandwidths are calculated from Fig. 13. The bandwidth of the single-pump FWM is 29.8 nm, while it is enhanced to 37.4 nm for the two-pump FWM. The bandwidth is improved by 25% through introducing the two-pump FWM regime.

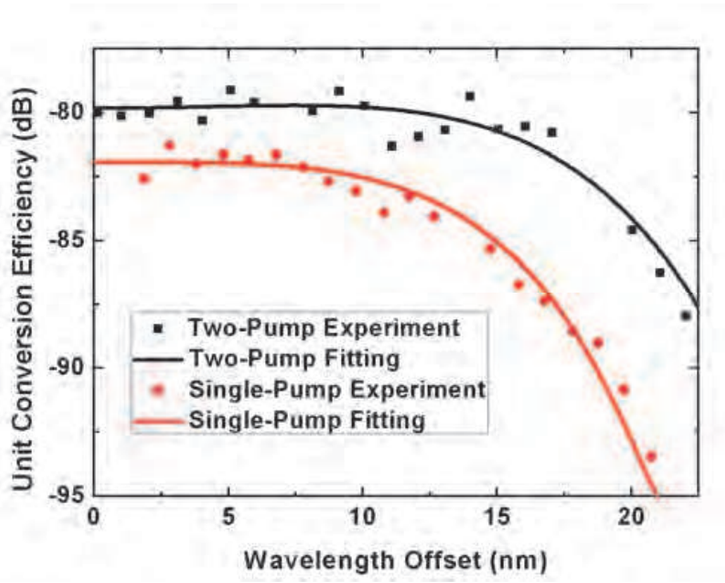


Fig. 13. Measured unit conversion efficiencies and the fitting curves for the two-pump and single-pump wavelength conversions. (Gao et al., 2010; © 2010 OSA)

3.2 Polarization independency

In a silicon nanowire waveguide, both the pump wave λ_p and the signal wave λ_s coupled into the waveguide can be decomposed to the TE and TM modes. FWM occurs only among these waves with the same polarization mode (Inoue, 1992). Under the law of energy conservation, the converted wave λ_c satisfies the relationship $1/\lambda_c = 2/\lambda_p - 1/\lambda_s$ for both TE- and TM-mode FWMs. By ignoring the pump and signal power transforms due to FWM and simplifying the coupled equations in Eqs. (1)-(3), the converted wave of TE or TM mode follows:

$$\frac{dA_{c-TE,TM}(z)}{dz} = -\frac{\alpha_{c-TE,TM}}{2} A_{c-TE,TM}(z) + j\gamma_{TE,TM} A_{p-TE,TM}^2(0) A_{s-TE,TM}^*(0) \times \exp\left[-\left(\alpha_{p-TE,TM} + \frac{\alpha_{s-TE,TM}}{2} + j\kappa_{TE,TM}\right) z\right] \tag{15}$$

where $A_{p,s,c\text{-}TE,\ TM}(z)$ are the amplitudes of the TE or TM mode of the pump, signal, and converted waves in the waveguide. Denoting the polarization angle of the incident pump or signal against the TE-axis as $\theta_{p,s}$, as shown in Fig. 14, the pump and signal fields coupled into the waveguide satisfy

$$\left|A_{p,s-TE}(0)\right| = \sqrt{C_{TE}} \left|A_{p0,s0}\right| \cos\theta_{p,s} \tag{16}$$

$$\left|A_{p,s-TM}(0)\right| = \sqrt{C_{TM}} \left|A_{p0,s0}\right| \sin\theta_{p,s} \tag{17}$$

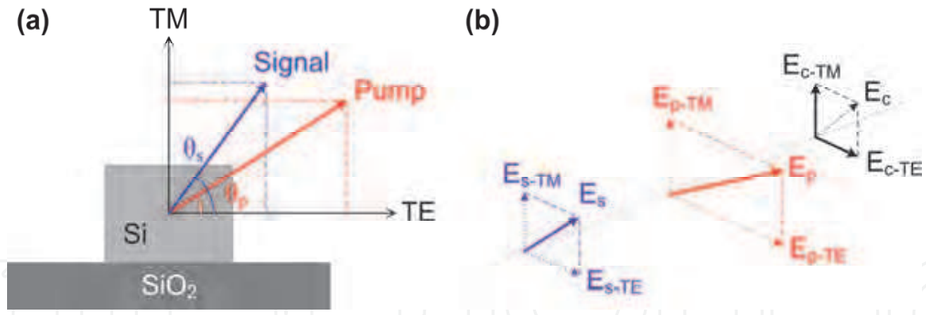


Fig. 14. Principle of the polarization-independent wavelength conversion based on FWM with an angled-polarization pump in a silicon nanowire waveguide. (a) Schematic description of the incident pump and signal; (b) FWM processes in the silicon nanowire waveguide. (Gao et al., 2010; © 2010 IEEE)

where $A_{p0,s0}$ are the amplitudes of the TE or TM mode of the incident pump and signal waves and $C_{TE,TM}$ is the relative coupling efficiency of the TE or TM mode. Assuming the incident pump and signal powers $P_{p0,s0} = |A_{p0,s0}|^2$, the coupled powers can also be written as

$$P_{p0,s0-TE} = C_{TE} P_{p0,s0} \cos^2 \theta_{p,s} \tag{18}$$

$$P_{p0,s0-TM} = C_{TM} P_{p0,s0} \sin^2 \theta_{p,s} \tag{19}$$

In Eq. (15), $\gamma_{TE,TM}$ is the nonlinear coefficient, $\kappa_{TE,TM}$ is the phase mismatch of the FWM process, and $a_{p,s,c\text{-}TE,TM}$ are the total losses of the pump, signal, and converted waves in the silicon nanowire waveguide, which are expressed as

$$\alpha_{p-TE,TM} = \alpha_{Lin-TE,TM} + \alpha_{TPA-TE,TM} + \alpha_{FCA-TE,TM} \tag{20}$$

$$\alpha_{s-TE,TM} = \alpha_{Lin-TE,TM} + 2\alpha_{TPA-TE,TM} + \alpha_{FCA-TE,TM} \tag{21}$$

$$\alpha_{c-TE,TM} = \alpha_{Lin-TE,TM} + 2\alpha_{TPA-TE,TM} + \alpha_{FCA-TE,TM} \tag{22}$$

Here $a_{Lin\text{-}TE,TM}$ is the linear loss coefficient of the TE or TM mode in the waveguide, and the TPA- and FCA-induced nonlinear loss coefficients are

$$\alpha_{TPA-TE,TM} = \beta_{TPA} P_{p0} \left(C_{TE} \cos^2 \theta_p + C_{TM} \sin^2 \theta_p \right) \Big/ A_{eff-TE,TM} \tag{23}$$

$$\alpha_{FCA-TE,TM} = \sigma \beta_{TPA} \tau_{eff} \lambda_p P_{p0}^2 \left(C_{TE} \cos^2 \theta_p + C_{TM} \sin^2 \theta_p \right)^2 \Big/ 2hcA_{eff-TE,TM}^2 \tag{24}$$

where β_{TPA} is the TPA coefficient, σ is the FCA cross section, τ_{eff} is the effective lifetime, h is the Planck's constant, and $A_{eff\text{-}TE,\,TM}$ is the effective mode areas for the TE or TM mode. The nonlinear coefficient $\gamma_{TE,\,TM}$ is expressed as

$$\gamma_{TE,TM} = 2\pi n_2 / \lambda_c A_{eff-TE,TM} \tag{25}$$

where n_2 is the nonlinear index coefficient. In the coupled equation, the TE- or TM-mode phase mismatch is

$$\kappa_{TE,TM} = \Delta\beta_{TE,TM} + 2\gamma_{TE,TM}\left[P_{p0-TE,TM} + \frac{2}{3}P_{p0-TM,TE}\right] \tag{26}$$

Denoting the wave numbers of the interaction waves as $\beta_{p,s,c}$, which can be calculated via the corresponding effective refractive indices $n_{p,s,c}$ in a silicon nanowire waveguide, the linear phase mismatch in Eq. (26) can be expressed as

$$\begin{aligned}\Delta\beta_{TE,TM} &= \beta_{s-TE,TM} + \beta_{c-TE,TM} - 2\beta_{p-TE,TM} \\ &= 2\pi\left(n_{s-TE,TM}/\lambda_s + n_{c-TE,TM}/\lambda_c - 2n_{p-TE,TM}/\lambda_p\right)\end{aligned} \tag{27}$$

The linear phase mismatch in Eq. (27) can also be rewritten using the dispersion values. Expanding $\beta_{p,s,c}$ in a Taylor series to the fourth-order around the pump wavelength λ_p, one obtains

$$\begin{aligned}\Delta\beta_{TE,TM} = &-\frac{1}{2\pi c}\left(\omega_s - \omega_p\right)^2 \lambda_p^2 D_{TE,TM}\left(\lambda_p\right) - \frac{1}{\left(2\pi c\right)^3}\left(\omega_s - \omega_p\right)^4 \\ &\times\left[\frac{1}{2}\lambda_p^4 D_{TE,TM}\left(\lambda_p\right) + \frac{1}{2}\lambda_p^5 D'_{TE,TM}\left(\lambda_p\right) + \frac{1}{12}\lambda_p^6 D''_{TE,TM}\left(\lambda_p\right)\right]\end{aligned} \tag{28}$$

where $D(\lambda_p)$ is the dispersion parameter at λ_p, $D'(\lambda_p)$ and $D''(\lambda_p)$ are the first- and second-order derivatives, respectively.
Solving Eq. (15) analytically, one obtains the generated converted wave:

$$\begin{aligned}A_{c-TE,TM}(L) = &\, j\gamma_{TE,TM} A_{p-TE,TM}^2(0) A_{s-TE,TM}^*(0) \\ &\times \exp\left(-\frac{\alpha_{c-TE,TM}L}{2}\right)\frac{1-\exp\left[\left(-j\kappa_{TE,TM} - \alpha_{p-TE,TM}\right)L\right]}{j\kappa_{TE,TM} + \alpha_{p-TE,TM}}\end{aligned} \tag{29}$$

The output converted power at the end of the waveguide can be expressed as

$$\begin{aligned}P_c(L) &= \left|A_{c-TE}(L)\right|^2 + \left|A_{c-TM}(L)\right|^2 \\ &= \gamma_{TE}^2 C_{TE}^3 P_{p0}^2 P_{s0}\exp\left(-\alpha_{c-TE}L\right)\left|\frac{1-\exp\left[\left(-j\kappa_{TE} - \alpha_{p-TE}\right)L\right]}{j\kappa_{TE} + \alpha_{p-TE}}\right|^2 \cos^4\theta_p \cos^2\theta_s \\ &+ \gamma_{TM}^2 C_{TM}^3 P_{p0}^2 P_{s0}\exp\left(-\alpha_{c-TM}L\right)\left|\frac{1-\exp\left[\left(-j\kappa_{TM} - \alpha_{p-TM}\right)L\right]}{j\kappa_{TM} + \alpha_{p-TM}}\right|^2 \sin^4\theta_p \sin^2\theta_s\end{aligned} \tag{30}$$

From Eq. (30) one sees that the converted wave power will be polarization-independent (i.e., independent of the SOP of the incident signal) when the following relationship is satisfied:

$$\left|\frac{1-\exp\left[\left(-j\kappa_{TE}-\alpha_{p-TE}\right)L\right]}{j\kappa_{TE}+\alpha_{p-TE}}\right| = \frac{\gamma_{TM}C_{TM}^{3/2}}{\gamma_{TE}C_{TE}^{3/2}}\tan^2\theta_p \times\exp\left[\frac{\left(\alpha_{c-TE}-\alpha_{c-TM}\right)L}{2}\right]\left|\frac{1-\exp\left[\left(-j\kappa_{TM}-\alpha_{p-TM}\right)L\right]}{j\kappa_{TM}+\alpha_{p-TM}}\right| \quad (31)$$

The incident pump polarization angle can be obtained by solving Eq. (31). Since the TE and TM phase mismatches and losses are also functions of the incident pump polarization angle, Eq. (31) can only be solved numerically. Substituting the solved pump polarization angle into Eq. (30), one can obtain the converted wave power for an arbitrary incident signal polarization angle and verify the polarization-independent characteristic.

Since the phase mismatch varies with the signal wavelength, the required pump polarization angle changes for different signal waves. Therefore, the polarization independence can be exactly realized only for one or several signal wavelengths once the pump polarization angle is determined, and the conversion efficiencies for the other signals will fluctuate slightly as the signal SOP varies. We take a 300 nm × 500 nm silicon nanowire waveguide as an example. The TE- and TM-polarization effective mode areas are $A_{eff\text{-}TE}$ = 9.484 × 10^{-2} μm² and $A_{eff\text{-}TM}$ = 9.838 × 10^{-2} μm². For convenience, the relative coupling efficiency of the TM mode is simplified as C_{TM} = 1, and the coupling efficiency ratio of the TE to TM mode is calculated to be C_{TE}/C_{TM} = 0.473 through mode filed overlapping integral method. This simplification does not affect the polarization-independent characteristic of the proposed wavelength conversion scheme. The linear propagation losses are considered as $a_{Lin\text{-}TE}$ = 2.5 dB/cm and $a_{Lin\text{-}TM}$ = 2 dB/cm for the TE and TM modes, the TPA coefficient is β_{TPA} = 0.5 cm/GW, the FCA cross section is σ = 1.45 × 10^{-17} cm², the effective lifetime of carriers is τ_{eff} = 2.5 ns, the nonlinear index coefficient is n_2 = 9 × 10^{-18} m²/W, and the waveguide length is L = 0.8 cm. According to Eq. (31), the required pump polarization angle is related to the losses and the phase mismatches of the TE and TM modes. Assuming the incident pump power is P_{p0} = 100 mW at wavelength λ_p = 1550 nm, the required pump polarization angle for each signal wavelength to realize exact polarization-independent wavelength conversion is obtained by substituting Eqs. (20)-(22) and (26) into Eq. (31), as shown in Fig. 15. It is noticeable that for a wide signal wavelength range the required pump polarization angles are almost the same. The inset shows the enlarged illustration in the range from 1530 to 1570 nm. The peak-to-peak fluctuation of the required pump polarization angles (for signals around the pump) is only 0.004° in the inset and the optimal pump polarization angle (averaged) is calculated to be 28.844°. One can use the average pump polarization angle in this region as the optimized value. This is of great convenience for the angled-polarization pump operation.

Figure 16(a) illustrates the conversion efficiency versus the signal wavelength. Here the shadowed region is used to illustrate the conversion efficiency fluctuation when changing the incident signal SOP arbitrarily, and the efficiency fluctuation is quantitatively described in Fig. 16(b). The enlarged description in the range from 1530 to 1570 nm is shown in the inset of Fig. 16(b), where one can find that four exact zero-fluctuation signal wavelengths exist, because the pump polarization angle we used here is exactly the solution of Eq. (31) for these signal wavelengths. In Fig. 16(b), one sees that the 1-dB polarization-independent bandwidth is 61 nm and the efficiency fluctuation is less than 0.04 dB for the signals in the

30-nm range around the 1550-nm pump. The wavelength conversion scheme we presented exhibits excellent polarization-independent characteristic in the entire C-band (the most significant telecommunication band) and thus is quite suitable for use in dense wavelength division multiplexing systems.

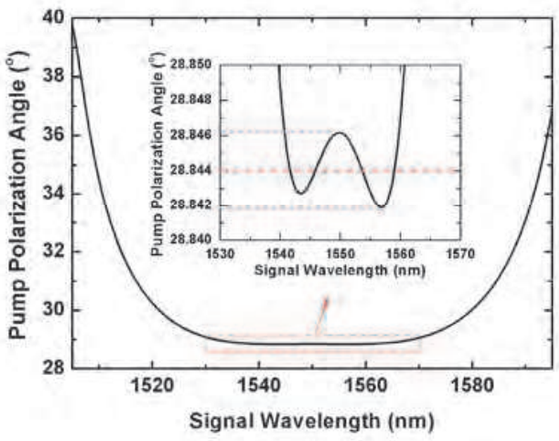


Fig. 15. Incident pump polarization angle required to realize exact polarization independence versus the signal wavelength in the 300 nm × 500 nm waveguide with a pump at 1550 nm. The inset shows the enlarged illustration in the range of 1530-1570 nm. (Gao et al., 2010; © 2010 IEEE)

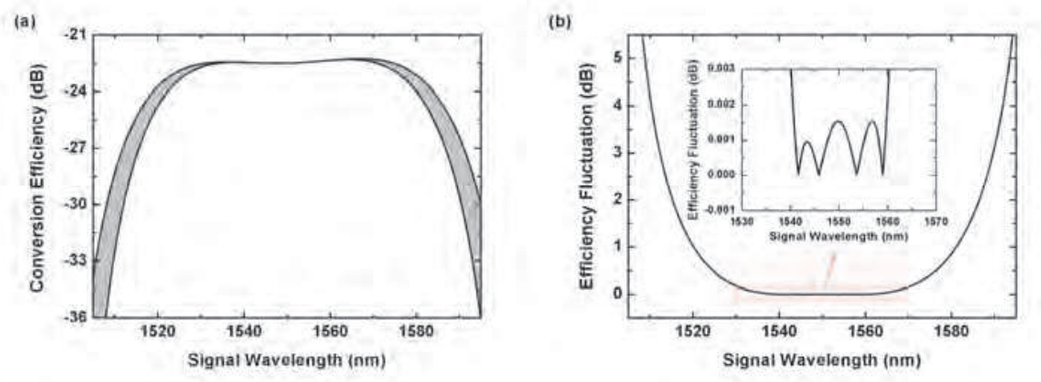


Fig. 16. (a) Conversion efficiency region and (b) the corresponding fluctuation value versus the signal wavelength. The inset in (b) shows the enlarged illustration in the range of 1530-1570 nm. (Gao et al., 2010; © 2010 IEEE)

For our proposed wavelength conversion scheme in silicon nanowire waveguides, the bandwidth is determined mainly by the TE- and TM-mode phase-matching conditions, which are related to the dispersions. The edges of these conversion efficiency regions in Fig. 16(a) are just the conversion efficiencies of the TE- and TM-polarization signals. Therefore, the polarization-independent bandwidth is limited by the larger one of the TE- and TM-mode phase mismatches, and the polarization-independent bandwidth is no more than the narrower one of the TE- and TM-mode bandwidths. If both the TE- and TM-mode

dispersion values in the 1550-nm band are reduced and flattened further by designing special waveguide structures and dimensions, larger polarization-independent bandwidth can be expected.

4. Summary and prospects

In this chapter, the FWM effect in silicon nanowire waveguides has been investigated and its applications in wavelength conversion have been introduced. The theoretical model of the FWM effect has been established. The conversion bandwidth and efficiency have been tried to improve by optimizing the waveguide geometry or designing special structure. Also, the improvement based on two-pump regime has been presented and demonstrated. The polarization independency of the wavelength conversion has been avoided by using an angled-polarization pump. Wavelength conversion based on silicon nanowire waveguides has been considered as a promising solution for the next generation integrated optical communication systems.

5. References

Fukuda, H. et al. (2005). Four-wave mixing in silicon wire waveguides. *Optics Express,* Vol.13, No.12, (June 2005), pp. 4629-4637, ISSN 1094-4087

Boyraz, O. & Jalali, B. (2004). Demonstration of a silicon Raman laser. *Optics Express,* Vol.12, No.21, (October 2004), pp. 5269-5273, ISSN 1094-4087

Liang, T. K. & Tsang, H. K. (2004). Efficient Raman amplification in silicon-on-insulator waveguides. *Applied Physics Letters,* Vol.85, No.16, (October 2004), pp. 3343-3345, ISSN 0003-6951

Almeida, V. R. et al. (2004). All-optical control of light on a silicon chip. *Nature,* Vol.431, No.7012, (October 2004), pp. 1081-1084, ISSN 0028-0836

Liang, T. K. et al. (2006). High speed logic gate using two-photon absorption in silicon waveguides. *Optics Communications,* Vol.265, No.1, (September 2006), pp. 171-174, ISSN 0030-4018

Foster, M. A. et al. (2006). Broad-band optical parametric gain on a silicon photonic chip. *Nature,* Vol.441, No.7096, (June 2006), pp. 960-963, ISSN 0028-0836

Rong, H. et al. (2006). High efficiency wavelength conversion of 10 Gb/s data in silicon waveguides. *Optics Express,* Vol.14, No.3, (February 2006), pp. 1182-1188, ISSN 1094-4087

Raghunathan, V. et al. (2005). Parametric Raman wavelength conversion in scaled silicon waveguides. *Journal of Lightwave Technology,* Vol.23, No.6, (June 2005), pp. 2094-2102, ISSN 0733-8724

Lin, Q. et al. (2006). Ultrabroadband parametric generation and wavelength conversion in silicon waveguides. *Optics Express,* Vol.14, No.11, (May 2006), pp. 4786-4799, ISSN 1094-4087

Sang, X. & Boyraz, O. (2008). Gain and noise characteristics of high-bit-rate silicon parametric amplifiers. *Optics Express,* Vol.16, No.17, (August 2008), pp. 13122-13132, ISSN 1094-4087

Zhang, X. et al. (2009). Optimal design of a silicon-on-insulator nanowire waveguide for broadband wavelength conversion. *Progress In Electromagnetics Research,* Vol.89, (January 2009), pp. 183-198, ISSN 1559-8985

Gao, S. et al. (2010). Performance Evaluation of Nondegenerate Wavelength Conversion in a Silicon Nanowire Waveguide. *Journal of Lightwave Technology,* Vol.28, No.21, (November 2010), pp. 3079-3085, ISSN 0733-8724

Foster, M. A. et al. (2007). Broad-band continuous-wave parametric wavelength conversion in silicon nanowaveguides. *Optics Express,* Vol.15, No.20, (September 2007), pp. 12949-12958, ISSN 1094-4087

Turner, A. C. et al. (2006). Tailored anomalous group-velocity dispersion in silicon channel waveguides. *Optics Express,* Vol.14, No.10, (May 2006), pp. 4357-4362, ISSN 1094-4087

Liu, Q. et al. (2011). Dispersion engineering of a silicon nanocrystal-based slot waveguide for broadband wavelength conversion. *Applied Optics,* in press, ISSN 1559-128X

Martínez, A. et al. (2010). Ultrafast all-optical switching in a silicon-nanocrystal-based silicon slot waveguide at telecom wavelengths. *Nano Letters,* Vol.10, No.4, (March 2010) pp. 1506-1511, ISSN 1530-6984

Gao, S. et al. (2010). Experimental demonstration of bandwidth enhancement based on two-pump wavelength conversion in a silicon waveguide. *Optics Express,* Vol.18, No. 26, (December 2010), pp. 27885-27890, ISSN 1094-4087

Inoue, K. (1992). Polarization effect on four-wave mixing efficiency in a single-mode fiber. *IEEE Journal of Quantum Electronics,* Vol.28, No.4, (April 1992), pp. 883-894, ISSN 0018-9197

Gao, S. et al. (2010). Polarization-independent wavelength conversion using an angled-polarization pump in a silicon nanowire waveguide. *IEEE Journal of Selected Topics in Quantum Electronics,* Vol.16, No.1, (January-February 2010), pp. 250-256, ISSN 1077-260X

IntechOpen



Nanowires - Fundamental Research

Edited by Dr. Abbass Hashim

ISBN 978-953-307-327-9
Hard cover, 552 pages
Publisher InTech
Published online 19, July, 2011
Published in print edition July, 2011

Understanding and building up the foundation of nanowire concept is a high requirement and a bridge to new technologies. Any attempt in such direction is considered as one step forward in the challenge of advanced nanotechnology. In the last few years, InTech scientific publisher has been taking the initiative of helping worldwide scientists to share and improve the methods and the nanowire technology. This book is one of InTechâ€™s attempts to contribute to the promotion of this technology.

How to reference

In order to correctly reference this scholarly work, feel free to copy and paste the following:

Shiming Gao and Sailing He (2011). Four-Wave Mixing in Silicon Nanowire Waveguides and Its Applications in Wavelength Conversion, Nanowires - Fundamental Research, Dr. Abbass Hashim (Ed.), ISBN: 978-953-307-327-9, InTech, Available from: http://www.intechopen.com/books/nanowires-fundamental-research/four-wave-mixing-in-silicon-nanowire-waveguides-and-its-applications-in-wavelength-conversion

INTECH
open science | open minds

InTech Europe
University Campus STeP Ri
Slavka Krautzeka 83/A
51000 Rijeka, Croatia
Phone: +385 (51) 770 447
Fax: +385 (51) 686 166
www.intechopen.com

InTech China
Unit 405, Office Block, Hotel Equatorial Shanghai
No.65, Yan An Road (West), Shanghai, 200040, China
中国上海市延安西路65号上海国际贵都大饭店办公楼405单元
Phone: +86-21-62489820
Fax: +86-21-62489821

© 2011 The Author(s). Licensee IntechOpen. This chapter is distributed under the terms of the Creative Commons Attribution-NonCommercial-ShareAlike-3.0 License, which permits use, distribution and reproduction for non-commercial purposes, provided the original is properly cited and derivative works building on this content are distributed under the same license.

IntechOpen

IntechOpen